Chapter 2

2.1. Introduction

In the recent era of science and technology, the nanocrystalline forms of the various systems such as ceramics, composites, intermetallics, and functionally-graded materials have attracted much attention from scientist, researchers and academicians due to potential application in the field of nano-science and technology, medical science and rich physics involved in these systems [Suib (2017); Abdal-hay et al. (2015); Yan et al. (2017); Manh et al. (2014)]. As we go from bulk system (macroscopic) to nano-scaled systems, in doped rare earth manganites, several interesting phenomena like disappearance of charge ordering, exchange bias effect, appearance of Griffiths Phase etc. are seen which are not shown by their bulk counterparts [Shankar et al. (2015); Giri et al. (2014a,b); Zhou et al. (2011)]. In the literature of science, several terms are found related to the nanomaterials such as nanoparticles, nanocrystals, nanotubes, nanorods, nanofibers and nanocomposites. Actually, all these terms are used some times interchangeably for the nanostructured materials. The physical and chemical behaviors of materials having particle sizes in the nanometer scale (typically 1-100 nm) are of gigantic curiosity and growing significance for future technological applications. Several techniques are used today to synthesize nanosized powder samples of ceramic oxides, such as sol-gel technique, hydrothermal synthesis and co-precipitation [Livage et al. (1989); Somiya et al. (2000); Kolthoff (1932)], spray drying, freeze drying, mechanical milling and so forth [Rahaman (1995)]. The solid state route, which is normally used for the synthesis of bulk ceramic powders, requires high sintering temperatures and longer time to obtain homogeneous composition. Hence, solid state route is unsuitable for synthesizing nano powders. Among the several techniques, combustion synthesis is one of the most efficient chemical route for synthesizing advanced nanomaterials, ceramics, intermetallics, composites, and functionally-graded

materials, which is also identified as self-propagating high-temperature synthesis (SHS) [Merzhanov et al. (1972); Ravindranathanan et al. (1986); Munir et al. (1989); Moore et al. (1995a,b); Hlavacek et al. (1996); Varma et al. (1998); Mukasyan et al. (2005); Chick et al. (1990)]. This method is used for the production of highly pure, uniformly distributed ceramic oxide powders. This method was discovered in the former Soviet Union by Merzhanov et al. (1972). This technique is adaptable for the production of a wide size range of ceramic systems [Patil et al. (2001)].

It offers several advantages such as,

(i) The initial reaction media being in the liquid state allows the homogeneous mixing of the reactants on the atomic level [Mukasyan et al. (2007)].

(ii) High reaction temperature for very short duration ensures high product purity and crystallinity, and on optimizing the parameters, allow us to synthesize the powders without the calcination step [Markovic et al. (2008)].

(iii) Short process duration and the formation of various gases during the combustion synthesis inhibits particle growth and favors the synthesis of nanopowders [Patil et al. (1997); Mukasyan et al. (2001); Patil et al. (2002); Varma et al. (2003); Deshpande et al. (2004)].

(iv) A comparative study of the effects of various synthesis techniques on the structure, particles size electrical and magnetic properties of manganites, showed that the combustion technique gave the smallest particle size and better homogeneity of the product [Conceicao et al. (2009a,b)].

In view of the above, all the samples investigated in the present thesis have been prepared by using combustion synthesis method. To get the nanocrystalline samples of various particle sizes and bulk samples, the as prepared combustion synthesized powders were annealed at various temperatures.

2.2. Basic Process of Combustion Synthesis

The combustion synthesis method involves a saturated aqueous acidic precursor solution of the required metal salts along with an appropriate organic fuel (such as glycine, urea, citric acid etc.) to boil until the mixture of the precursor ignites, and a self-supporting and somewhat quick combustion reaction takes place, resulting usually crystalline, and a dry and fine powder [Fumo et al. (1997)]. To synthesize a complex mixed oxide, a combination of the precursor containing required metal ions in the form of quickly soluble salts in water (for example nitrate salts) and a fuel for instance glycine or urea or citric acid can be used [Mukasyan et al. (2001); Patil et al. (2001); Patil et al. (2002)]. While such types of redox reactions are exothermic, and normally an uncontrolled reaction may lead to the explosion if larger quantity of reactants are used. The combustion of metal nitrates-organic fuel mixtures typically takes place as a self-propagating and nonexplosive exothermic reaction for smaller quantities. A large amount of gases generated during the auto-ignition process can result in the form of the flame, which can achieve temperatures over 1000°C for a very short duration. The fuels which are used serve two purposes:

a) They are sources of H and C which on combustion will form CO_2, H_2O and release heat.
b) They form complexes with the metal ions facilitating uniform mixing of the cations in solution.

By simple calcination, the metal nitrates are disintegrated into metal oxides upon heating to or above the phase conversion temperature. A stable external heat source is essential in this case; to keep the system at the high temperature necessary for achieving the suitable phase transition or decomposition. In combustion synthesis technique, the energy liberated from the exothermic reaction among the nitrates and the organic fuel,

which generally catches fire can quickly heat the system to the high temperature and maintain it long enough, for production to take place.

2.3. Basic Principles of Calculations in Combustion Synthesis

The basic concept of the combustion synthesis methods appears from the notions of thermochemistry used in the area of explosives and propellants. A clear indication of the efficient constitutions of fuel and oxidizer mixture is necessary for the calculation to balance the oxidizing and reducing valances in the system. Jain et al. (1981) developed an easiest method of estimating the reducing to oxidizing nature of the mixture. This technique consists of generating a straightforward valency balance method, irrespective of whether the elements are present in the fuel/reducer or the oxidizer parts of the combination, to compute the stoichiometric composition of the redox combination which corresponds to liberate the maximum energy for the combustion reaction. The considered valences are those assumed by the elements in the common products of the combustion reactions, which are CO_2, H_2O and N_2. Hence, the elements carbon (C) and hydrogen (H) are supposed as reducing elements with the analogous valencies +4 and +1, respectively, whereas, oxygen (O) is supposed as an oxidizing element having the valency -2 and nitrogen (N) is considered as an element having valency zero. In the combustion reaction, as oxidizers, metal nitrates are favored, since they are water soluble, and a few hundred degrees is sufficient for their decomposition. The total valency in many divalent nitrates is -10 and in trivalent nitrates is -15. Also, it has been found that the most privileged products of combustion synthesis technique accompanied with nitrates are, definitely, N_2 and O_2 [Fumo et al. (1996)].

Once we calculate the amounts of the nitrates salts and the glycine to be used in the process, we can write down the different chemical reactions that might be engaged in the process, and calculate the enthalpy of the reaction [Silbey et al. (2000)], using the relation $\Delta H^\circ = (\Sigma\ n.\ \Delta H_f^\circ)_{products} - (\Sigma\ n.\ \Delta H_f^\circ)_{reactants}$ where, n is the number of moles and ΔH° is the enthalpy of the reaction.

2.4. Characterization Techniques

2.4.1. X-ray Diffraction (XRD) of Powder Samples

X-ray diffraction is a powerful and non-destructive technique used to characterize materials based on their own unique pattern. One can also identify the nature of crystallinity (crystalline, amorphous, semi-crystalline, polymer etc.) of the materials using XRD patterns of materials. X-ray diffraction pattern can be used to uniquely solve the crystal structure of the materials having single or multiple phases by Rietveld structure refinement [Young (1993)] and phase fractions of various phases can be determined within the material. The powder diffraction patterns are the characteristic of the given materials and each material generates its own diffraction pattern which is different from any other material similar to human finger print. The great advantage of powder X-ray diffraction technique is that it can also be used in the chemical analysis, stress measurement, study of phase equilibrium, determination of particle size, strain and in-situ measurements. In the present works, the calcined powders were characterized for structure and phase analysis using powder X-ray diffraction measurements. The XRD measurements were carried out using Benchtop Miniflex600 (Rigaku, Japan) powder X-ray diffractometer having $Cu_{K\alpha}$ target working in the Bragg-Brentano geometry and fitted with a graphite monochromator within the diffracted beam in the 2θ range of 20°-120° with a scan rate of 2°/min. High resolution XRD

measurements were also done using Rigaku SmartLab system having $Cu_{K\alpha 1}$ optics with Johansson monochromator.

2.4.2. Scanning Electron Microscopy

Scanning electron microscopy (SEM) is an important and non-destructive tool to analyze the surface morphology of metallic, semiconducting and insulating materials by taking magnified images. A SEM scans uses a focused accelerated electron beam instead of visible light over the surface of materials to generate an image. The accelerated electrons in the beam interact with the material, generating a variety of signals that can be used to acquire information about the surface topography and composition of the sample. The stream of electrons is produced by an electron gun and is accelerated from few 100 eV to 40 keV of energy. The electron beam tracks a vertical path throughout the microscope, which is held within high vacuum. The beam is focused using magnetic lenses to a spot size of about 0.4 to 5 nm in diameter on the surface of sample. Once the beam hits on the surface of the sample, X-rays, backscattered electrons and secondary electrons emerge from it. Detectors accumulate these X-rays, secondary electrons, backscattered electrons and transfer them into an image/signal that can be visualized on a computer screen. The electron beam is scanned across the sample through magnetic scan coils. The current produced due to the backscattered electrons is accumulated, amplified and plotted as a 2D 'micrograph' image of the signal. For recording of the SEM micrograph, samples should be conducting to ensure no charging from incident electrons during the measurement. The samples are mounted on the sample holder using carbon tapes or conducting paste.

For the present study, a scanning electron microscopy (SEM) (Evo Research 18, ZEISS), and high resolution scanning electron microscop (HR-SEM) (Nova NanoSEM 450, FEI) equipped with energy dispersive X-ray spectroscopy (EDS) technique were

used for recording the micrographs. The Ti-doped $R_{1-y}Ba_yMn_{1-x}Ti_xO_3$ (R = La, Nd) manganites were coated with conducting gold layer by sputtering under vacuum before recording the micrographs to avoid charging of the samples. The gun voltage was varied to capture well focused micrographs of the sample. Elemental and compositional analyses were performed by the EDS technique available with the above systems. Its working principle is that each element has a unique atomic structure which allows emission of X-rays at the characteristic energy levels that provides a characteristic unique peak in the spectra for each element which is distinguishable from the X-rays emitted by another element. Further, the EDS technique can be used for qualitative (type of elements) as well as quantitative (percentage of concentration of each element) analysis.

2.4.3. Magnetic Measurements

Magnetic measurements are done to know the magnetic state of a material. The fundamental measurements include the measurement of magnetization as a function of temperature with a constant probing magnetic field. Magnetization measurements as a function of applied external magnetic field at constant temperature also facilitate to get the magnetic behavior of the material. Sometimes temperature and frequency dependence of magnetization measurements also help to know the dynamic behavior of the magnetic systems. In this work for magnetic characterizations, we used a commercial vibrating sample magnetometer (VSM) (MPMS3 from Quantum Design, USA), a superconducting quantum interference device (SQUID: MPMS from Quantum Design, USA) and superconducting quantum interference device - vibrating sample magnetometer (SQUID-VSM from Quantum Design, USA).

The facilities were utilized from Central Instrumental Facility (CIF), Indian Institute of Technology (BHU), Varanasi, India. Brief descriptions of the working principle of these systems are given below.

2.4.3.1. Vibrating Sample Magnetometer (VSM)

The dc magnetization measurements of Ti-doped $R_{1-y}Ba_yMn_{1-x}Ti_xO_3$ (R = La, Nd) nanocrystalline and microcrystalline manganites were carried out using a commercial VSM having specification for temperature variation from 2-400 K and magnetic field ± 70 kOe (7 Tesla). For the measurement of magnetic moment, a VSM involves induction method that refers to the measurement of electromotive force (emf) (voltage) induced in a set of detection (pickup) coils by a varying magnetic moment. In this process, sample under investigation is vibrated in a uniform magnetic field, which induces voltage at the detection coil. For instance, if a magnetic dipole, initially placed in the center of a pickup (detection) coil, is moved to a distance then a flux (Φ) is produced which results in inducing an emf ($e = d\Phi/dt$) in the detection coil. The pickup coils may be located inside a solenoid (for generating magnetic field), so that the moment can be measured as a function of the externally applied magnetic field [Foner (1959)].

2.4.3.2. SQUID Magnetometer

The SQUID magnetometer is a most susceptible apparatus available to measure the magnetization or magnetic field. However, it does not measure the magnetic field from the sample directly. For the measurement of the magnetic field, the sample is made to move through superconducting detection coils coupled to the SQUID through superconducting wires, allowing the current from the detection coils to inductively coupled to SQUID sensor. The basic function of a SQUID is to convert current in to voltage sensibly. The instrument essentially contains the following parts: the SQUID

(main unit of the device), a magnetic flux transformer including pickup (or detection) coils, the superconducting magnetic coil, magnetic shielding and heat switches. The superconducting pickup coils are constructed as a second-order gradiometer (used for measuring magnetic field gradient), with counter-wound outer loops which make the set of coils non-responsive to linear magnetic field gradients and uniform magnetic fields. The detection coils only produce a current in response to the local magnetic field disturbances [Clarke (1996)]. The superconducting magnetic coils are used to apply large magnetic fields. Since SQUID is extremely sensitive to minute fluctuations of the magnetic field, magnetic shielding is inevitable to shield the sensor itself both from the large magnetic fields created by the superconducting coil and the fluctuations in the ambient magnetic field of the laboratory. Heaters are employed to heat up the small section of the detection coil circuit whenever the magnetic field is altered. They permit for the removal of standing currents in the superconducting loops by heating them above their critical temperature.

2.4.3.3. SQUID–Vibrating Sample Magnetometer (SQUID-VSM)

The SQUID-VSM is a modified version of SQUID magnetometer. It measures the magnetic moment of the magnetic sample by combining the speed of a VSM and the sensitivity of a SQUID. The magnetic sample is vibrated at a known frequency and phase-sensitive detection is utilized for quick data compilation and rejection of unauthentic signals. Here, it is worth noting that the sample vibration is anyhow not the essential requirement to produce the signal as in a conventional copper-pickup-coil VSM, where a changing magnetic flux is necessary. Instead, the sample vibration is used only to generate a signal at a recognized modulation frequency to assist the separate out the sample signals from the instrumental artifacts. The size of the signal does not depend on the vibration frequency and higher vibration frequencies will not

improve the signal to noise ratio, as in a conventional VSM. This is because of the use of superconducting detection coils which produces a current in response to magnetic flux, rather than to a change in magnetic flux as manufactured by copper coils.

2.5. Doped Manganite Sample Preparation using Auto-combustion Method

2.5.1. Synthesis of $Nd_{1-y}Ba_yMn_{1-x}Ti_xO_3$ (y = 0.30) Manganites

The polycrystalline $Nd_{0.70}Ba_{0.30}Mn_{1-x}Ti_xO_3$ ($0.0 \leq x \leq 0.50$) perovskite manganites with nominal compositions were prepared by the glycine-nitrate auto-combustion method [Kumar et al. (2019)]. The stoichiometric amounts of Nd_2O_3 (99.0%, Sigma Aldrich), $BaCO_3$ (99.9%, Sigma Aldrich), $Mn(CH_3COO)_2.4H_2O$ (99.0%, Sigma Aldrich), and titanium isopropoxide ($Ti[OCH(CH_3)_2]_4$, 97.0%, Sigma Aldrich) were used as reactants. The stoichiometric amounts of the redox mixture for combustion was estimated on the basis of the total reducing and oxidizing valences of the oxidizer (O) and the fuel (F), where O and F worked as numerical coefficients so that the equivalence ratio φ_c (O/F), turned into unity [Singh et al. (2006)]. Using the concept of propellant chemistry, the valence C = +4, Ti = +4, Nd = +3, Ba = +2, Mn = +2, H = +1, N = 0 and O = -2 has been considered to calculate the amount of reactants for combustion synthesis. The stoichiometric amounts of Nd_2O_3 and $BaCO_3$ were weighed and dissolved in dilute nitric acid (dil. HNO_3 69.0%, Hi-media) to form nitrates and the stoichiometric amounts of $Mn(CH_3COO)_2.4H_2O$ and glycine ($C_2H_5NO_2$, 99.5%, Hi-media) were dissolved in distilled water to form precursors solution, while the stoichiometric amount of titanium isopropoxide was stabilized in ethylene glycol. All the reactant precursor solutions and aqueous solution of the fuel (here, glycine) were mixed in a large beaker with capacity of five liters. Then the resulting solution was kept on a magnetic hot plate at 200°C under constant stirring. As time increases, the

precursor solution gets thicker due to evaporation of the aqueous solution. After 6-8 hrs of continuous stirring and heating finally auto-ignition take place and whole solution converted into blackish-brown colored powder. After auto-combustion the blackish-brown powder was collected from the beaker. The obtained powder was divided into numerous parts which were calcined at different temperatures for 6 hrs to get the phase pure samples of various particle sizes. **Fig. 2.1** displays schematic diagram for the synthesis of $Nd_{0.70}Ba_{0.30}Mn_{1-x}Ti_xO_3$ ($0.0 \leq x \leq 0.50$) manganites.

The as prepared sample (just after combustion) of $Nd_{0.7}Ba_{0.3}MnO_3$ manganite was calcined at 700, 800, 900, 1000, 1100 and 1200°C. The XRD patterns for all the samples collected in the 2θ range 20-80° with a scan rate of 2°/min are shown in **Fig. 2.2**. The XRD patterns show presence of some impurity phases below 1200°C temperature and at 1200°C it display formation of pure single phase. Hence, the Ti-doped samples of $Nd_{0.70}Ba_{0.30}Mn_{1-x}Ti_xO_3$ with $0.0 \leq x \leq 0.30$ were calcined at 1200°C, while the samples with x = 0.40 and 0.50 were calcined at 1350°C for 6 hrs to achieve the higher phase purity. **Fig. 2.3** shows RT XRD patterns for $Nd_{0.70}Ba_{0.30}Mn_{1-x}Ti_xO_3$ manganites.

Calculation of Stoichiometric Amount of Raw Materials for the synthesis of 5 gm $Nd_{0.7}Ba_{0.3}Mn_{1-x}Ti_xO_3$ Manganites

Molecular Weight of $Nd_{0.7}Ba_{0.3}Mn_{1-x}Ti_xO_3$:

= 0.7 × 144.242 + 0.3 × 137.327 + (1-x) × 54.938 + (x) × 47.867 + 3 × 15.9994

= 245.1037 - 7.071*x*

= Z gm/mol

(1) Nd_2O_3 = 336.48 gm/mol

$$\text{Required amount} = \frac{0.7 \times 336.48 \times 5}{2 \times Z} = y_1 \text{ gm}$$

(2) $BaCO_3$ = 197.34 gm/mol

$$\text{Required amount} = \frac{0.3 \times 197.34 \times 5}{Z} = y_2 \text{ gm}$$

(3) $Mn(CH_3COO)_2.4H_2O$ = 245.09 gm/mol

$$\text{Required amount} = \frac{(1 - x) \times 245.09 \times 5}{Z} = y_3 \text{ gm}$$

(4) Titanium isopropoxide = 284.219 gm/mol

$$\text{Required amount} = \frac{x \times 284.219 \times 5}{Z} = y_4 \text{ gm}$$

Assay Corrections:

(1) $Nd_2O_3 = y_1 \times 100 / 99 =$ **y_1' gm**

(2) $BaCO_3 = y_2 \times 100 / 99 =$ **y_2' gm**

(3) $Mn(CH_3COO)_2.4H_2O = y_3 \times 100 / 99 =$ **y_3' gm**

(4) Titanium isopropoxide = $y_4 \times 100 / 97 =$ **y_4' gm**

Calculation of amount of Fuel (Glycine) Used during Synthesis Process:

Total valence of various reactants:

$0.7\ Nd(NO_3)_3 = 0.7 \times (+3 + 3 \times 0 - 2 \times 9) = - 10.5$

$0.3\ Ba(NO_3)_2 = 0.3 \times (+2 + 2 \times 0 - 2 \times 6) = - 3$

$(1\text{-}x)\ Mn(CH_3COO)_2.4H_2O = (1\text{-}x)\ (+2 + 4 \times 4 + 6 \times 1 - 4 \times 2) = + 16\ (1\text{-}x)$

$x\ Ti\{OCH(CH_3)_2\}_4 = x\ (+4 - 4 \times 2 + 12 \times 4 + 28 \times 1) = + 72\ x$

$C_2H_5NO_2 = (2 \times 4 + 5 + 0 - 2 \times 2) = + 9$

Balancing Oxidizing and Reducing agents for combustion:

$[16\ (1\text{-}x) + 72\ x + 9]\ n - [10.5 + 3] = 0$

Or, $n = 13.5 / (25 + 56\ x)$

Here, $n = n_1 + n_2 + n_3$

Where, $n_1 = y_3' / 245.09$ mol, $n_2 = y_4' / 284.219$ mol, and $n_3 = n - n_1 - n_2$

(5) $C_2H_5NO_2$ = 75.07 g/mol

$$\text{Required amount} = \frac{n_3 \times 75.07 \times 100}{99.5} = \mathbf{y_5'\ gm}$$

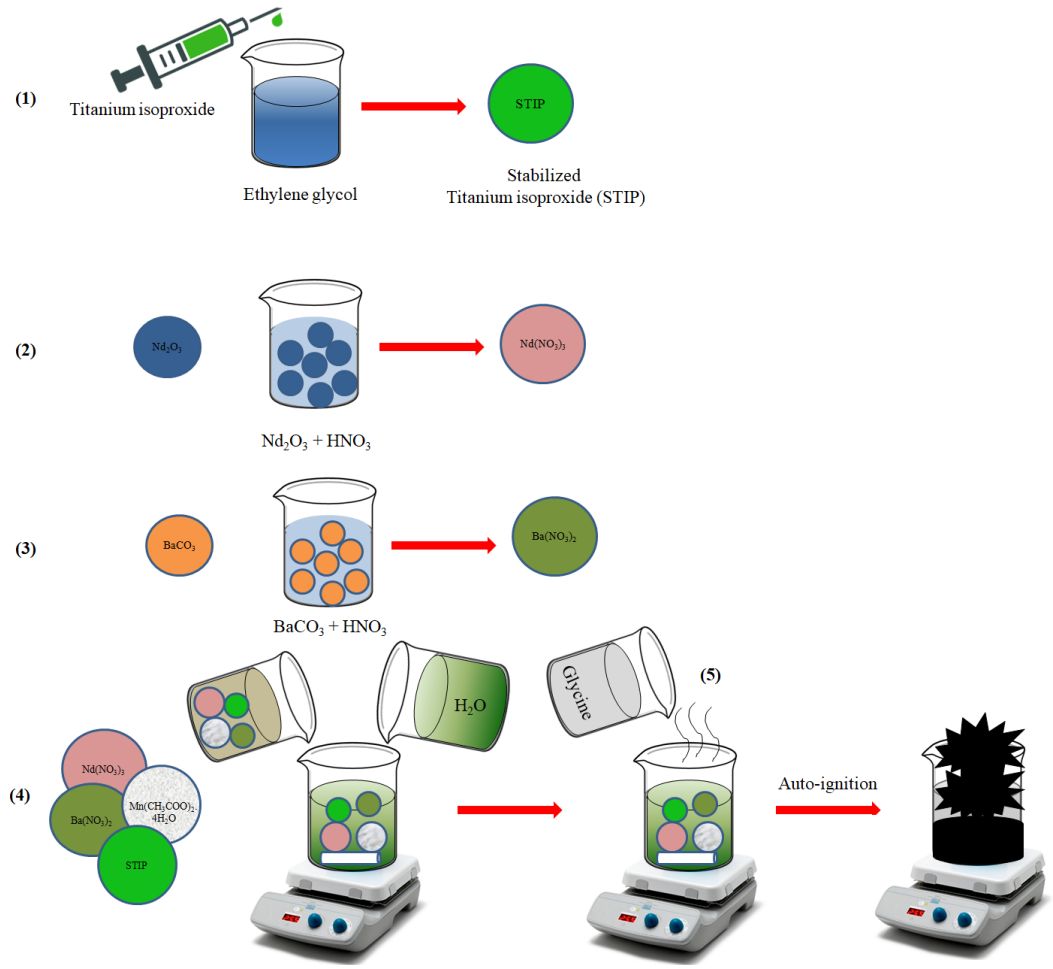

Figure 2.1: Schematic diagram of process for the synthesis of $Nd_{0.7}Ba_{0.3}Mn_{1-x}Ti_xO_3$ ($0.0 \leq x \leq 0.50$) perovskite manganites.

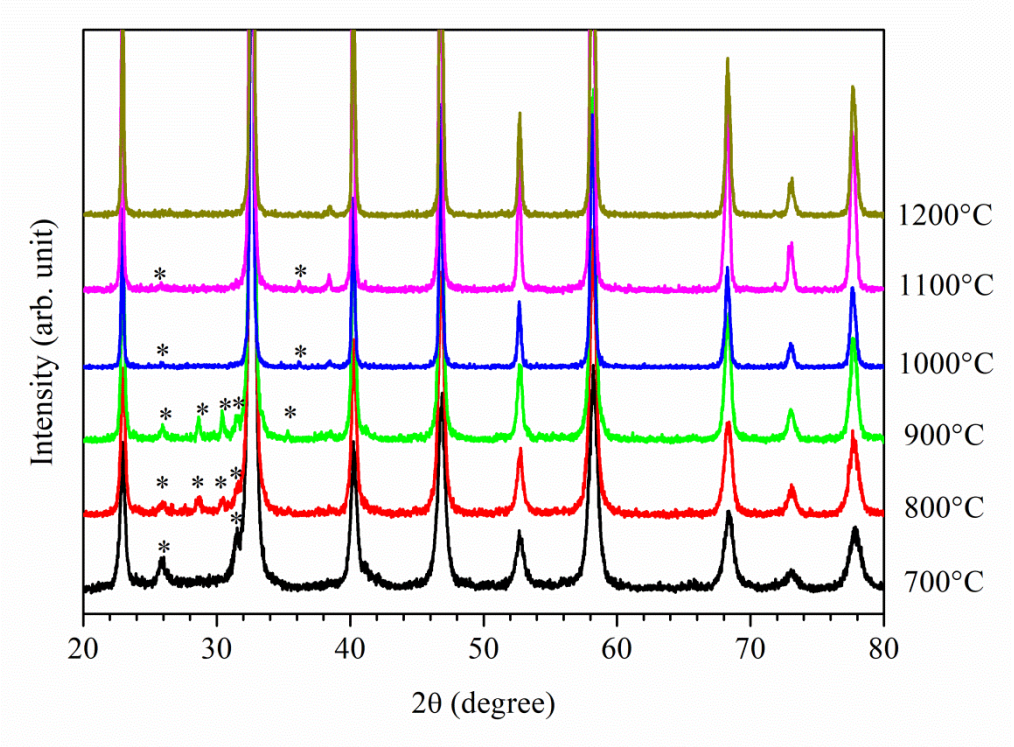

Figure 2.2: The room temperature XRD patterns of $Nd_{0.7}Ba_{0.3}MnO_3$ manganite calcined at various temperatures.

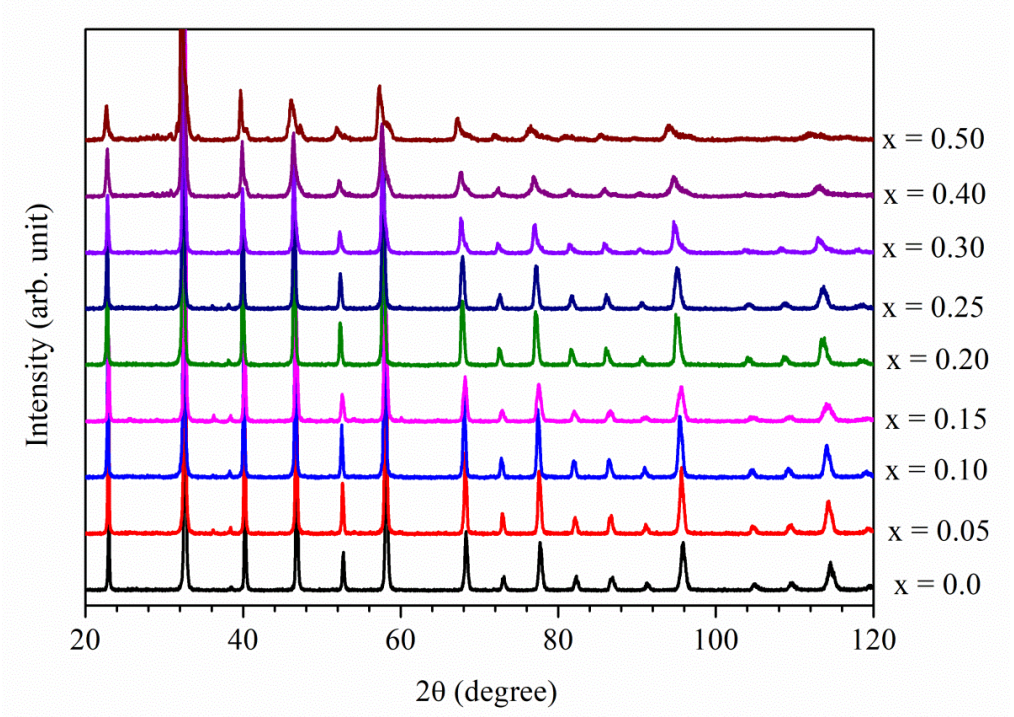

Figure 2.3: The room temperature XRD patterns of $Nd_{0.7}Ba_{0.3}Mn_{1-x}Ti_xO_3$ ($0.0 \leq x \leq 0.50$) perovskite manganites prepared at optimized temperatures.

As shown in **Fig. 2.4**(a), the XRD pattern for NBMO-30 manganite can be indexed with *Imma* space group of orthorhombic structure. The structural analysis was performed by Rietveld refinement of the XRD pattern to confirm the structure. **Fig. 2.4**(b) shows Rietveld fit for NBMO-30 manganite calcined at 1200°C, in which solid scattered dot points are used to show observed XRD pattern and continuous line over observed pattern represents calculated pattern; lower curve represents difference between observed and calculated XRD patterns and vertical bars show positions of Bragg's peaks. We estimated average values of lattice strain and crystallite size using Williamson-Hall plot technique (Kumar et al. (2018a) and found that crystallite size increases linearly and lattice strain decreases non-linearly with enhancing calcination temperature as shown in **Fig. 2.4**(c). **Fig. 2.4**(d) shows variation in unit cell volume with crystallite size for NBMO-30 manganite [Kumar et al. (2018b)].

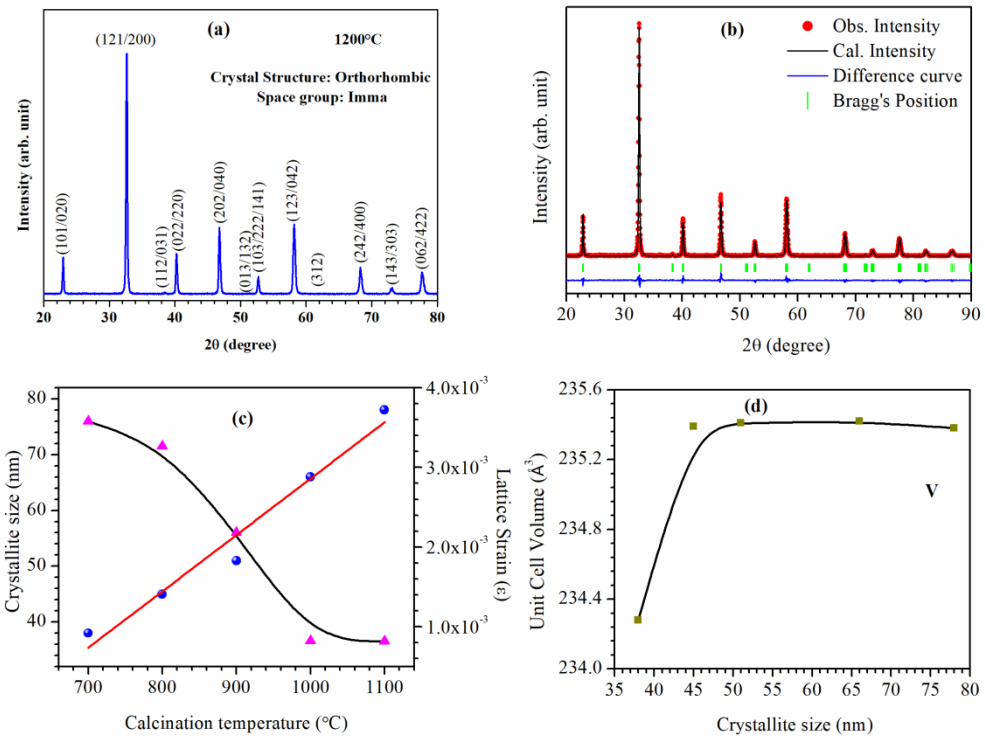

Figure 2.4: (a) XRD pattern and its (b) Rietveld fit for NBMO-30 calcined at 1200°C. (c) Variation of crystallite size and lattice strain with calcination temperature. (d) Variation in unit cell volume with crystallite size.

The $Nd_{0.7}Ba_{0.3}Mn_{1-x}Ti_xO_3$ manganite with x = 0.10 was also calcined at different temperatures i.e., at 800, 900, 1000 and 1100°C for 6 hrs. We recorded their XRD patterns from 2θ = 20° to 2θ = 120° with a step size of 0.02° at a scan rate of 2°/min. **Fig. 2.5** displays the RT XRD for $Nd_{0.7}Ba_{0.3}Mn_{0.90}Ti_{0.10}O_3$ manganite calcined at various temperatures. As can be seen from this figure phase pure samples can be obtained relatively at lower temperature than the samples without Ti-substitution.

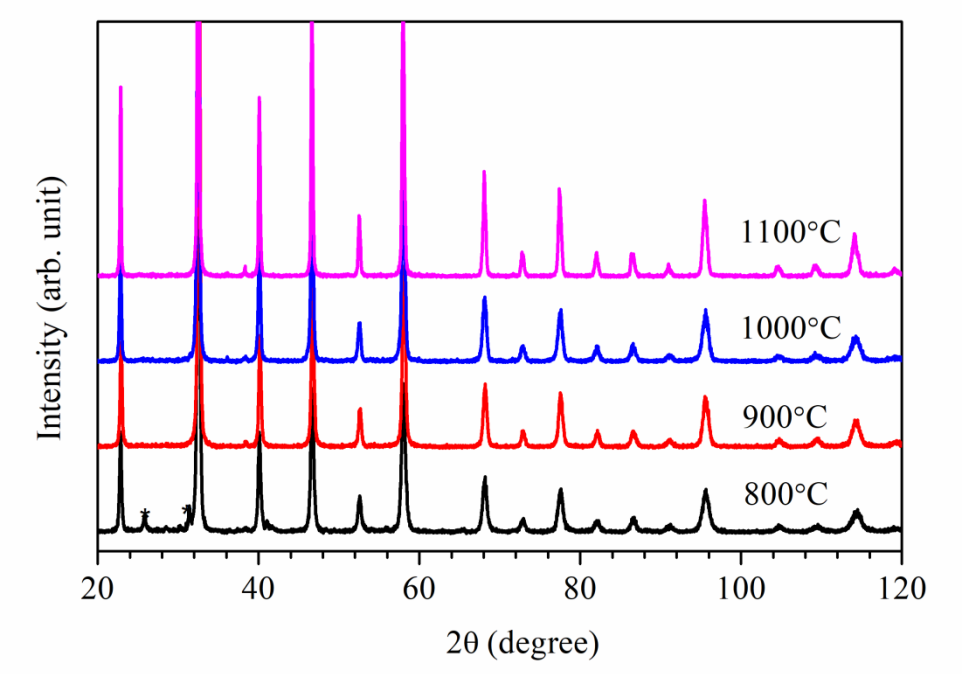

Figure 2.5: Room temperature XRD patterns of $Nd_{0.7}Ba_{0.3}Mn_{1-x}Ti_xO_3$ manganite with x = 0.10 calcined at several temperatures from 800 to 1100°C.

2.5.2. Synthesis of $La_{1-y}Ba_yMn_{1-x}Ti_xO_3$ (y = 0.40) Manganites

The polycrystalline $La_{0.60}Ba_{0.40}Mn_{1-x}Ti_xO_3$ ($0.0 \leq x \leq 0.20$) perovskite manganites with nominal compositions were also prepared by the glycine-nitrate auto-combustion method discussed above. The lanthanum oxide (La_2O_3, 99.9 %, Sigma Aldrich), barium carbonate ($BaCO_3$, 99.0%, Sigma Aldrich), manganese acetate hexahydrate ($Mn[CH_3COO]_2.4H_2O$, 99.0%, Sigma Aldrich), and titanium isopropoxide

($Ti[OCH(CH_3)_2]_4$, 97.0%, Sigma Aldrich) were used as reactants. The stoichiometric amounts of the redox mixture for combustion was estimated on the basis of the total reducing and oxidizing valences of the oxidizer (O) and the fuel (F), where O and F worked as numerical coefficients so that the equivalence ratio φ_c (O/F), becomes unity [Singh et al. (2006)]. Using the concept of propellant chemistry, the valence C = +4, Ti = +4, La = +3, Ba = +2, Mn = +2, H = +1, N = 0 and O = -2 has been considered to calculate the composition for combustion synthesis as discussed earlier. The required stoichiometric amounts of La_2O_3 and $BaCO_3$ were dissolved in dilute nitric acid (dil. HNO_3 69.0 %, Hi-media) to convert into nitrates and the stoichiometric amounts of $Mn(CH_3COO)_2.4H_2O$ and glycine ($C_2H_5NO_2$, 99.5 %, Hi-media) were dissolved in distilled water to form precursors solution, while the stoichiometric amount of titanium isopropoxide was stabilized in ethylene glycol. All the reactant precursor solutions and aqueous solution of the fuel (here, glycine) were mixed a large beaker with capacity of five liters. Then the resulting solution was kept on a magnetic hot plate at 225°C under constant stirring. As time increases, the precursor solution gets thicker due to evaporation of the aqueous solution. After 5-6 hrs of constant stirring finally auto-ignition take place and whole solution converted into blackish-brown colored powder. After auto-combustion the blackish-brown powder was collected from the beaker and calcined at 1300°C temperature for 6 hrs. The whole processes of the synthesis of $La_{0.6}Ba_{0.4}Mn_{1-x}Ti_xO_3$ manganites are presented schematically in **Fig. 2.6**. The room temperature powder XRD patterns for the $La_{0.6}Ba_{0.4}Mn_{1-x}Ti_xO_3$ manganites with $0.0 \leq x \leq 0.20$ are shown in **Fig. 2.7**. Phase identification and characterization of the synthesized materials was carried out by Rietveld analysis of XRD patterns. $La_{0.6}Ba_{0.4}Mn_{1-x}Ti_xO_3$ manganites crystallize into single phase of cubic crystal structure with $Pm\bar{3}m$ space group. **Fig. 2.8**(a) show Rietveld fit between observed and calculated

XRD patterns for $La_{0.6}Ba_{0.4}Mn_{1-x}Ti_xO_3$ manganite with x = 0. Rietveld analysis shows that the unit cell volume for $La_{0.6}Ba_{0.4}Mn_{1-x}Ti_xO_3$ manganites increases with increasing doping concentration of Ti^{4+}-ion. **Fig. 2.8**(b) displays variation in unit cell volume for $La_{0.6}Ba_{0.4}Mn_{1-x}Ti_xO_3$ manganites as a function of Ti^{4+}-doping concentration (x).

Calculation of Stoichiometric Amount of Raw Materials for the synthesis of 5 gm $La_{0.6}Ba_{0.4}Mn_{1-x}Ti_xO_3$ Manganites:

Molecular Weight of $La_{0.6}Ba_{0.4}Mn_{1-x}Ti_xO_3$:

$= 0.6 \times 138.9055 + 0.4 \times 137.327 + (1-x) \times 54.938 + (x) \times 47.867 + 3 \times 15.9994$

$= 241.2103 - 7.071x$

$= Z$ gm/mol

(1) La_2O_3 = 325.81 gm/mol

$$\text{Required amount} = \frac{0.6 \times 325.81 \times 5}{2 \times Z} = x_1 \text{ gm}$$

(2) $BaCO_3$ = 197.34 gm/mol

$$\text{Required amount} = \frac{0.4 \times 197.34 \times 5}{Z} = x_2 \text{ gm}$$

(3) $Mn(CH_3COO)_2.4H_2O$ = 245.09 gm/mol

$$\text{Required amount} = \frac{(1-x) \times 245.09 \times 5}{Z} = x_3 \text{ gm}$$

(4) Titanium isopropoxide = 284.219 gm/mol

$$\text{Required amount} = \frac{x \times 284.219 \times 5}{Z} = x_4 \text{ gm}$$

Assay Corrections:

(1) $La_2O_3 = x_1 \times 100 / 99.9 =$ **x_1' gm**

(2) $BaCO_3 = x_2 \times 100 / 99 =$ **x_2' gm**

(3) $Mn(CH_3COO)_2.4H_2O = x_3 \times 100 / 99 =$ **x_3' gm**

(4) Titanium isopropoxide = $x_4 \times 100 / 97 =$ **x_4' gm**

Calculation of amount of Fuel (Glycine) Used during Synthesis Process:

Valence: $0.6\ La(NO_3)_3 = 0.6 \times (+3 + 3 \times 0 - 2 \times 9) = -9$

$0.4\ Ba(NO_3)_2 = 0.4 \times (+2 + 2 \times 0 - 2 \times 6) = -4$

$(1-x)\ Mn(CH_3COO)_2.4H_2O = (1-x)\ (+2 + 4 \times 4 + 6 \times 1 - 4 \times 2) = +16\ (1-x)$

$x\ Ti\{OCH(CH_3)_2\}_4 = x\ (+4 - 4 \times 2 + 12 \times 4 + 28 \times 1) = +72\ x$

$C_2H_5NO_2 = (2 \times 4 + 5 + 0 - 2 \times 2) = +9$

Balancing Oxidizing and Reducing agents for combustion:

$[16\ (1-x) + 72\ x + 9]\ n - [9 + 4] = 0$

Or, $n = 13 / (25 + 56\ x)$

Here, $n = n_1 + n_2 + n_3$

Where, $n_1 = x_3 / 245.09$ mol, $n_2 = x_4 / 284.219$ mol, and $n_3 = n - n_1 - n_2$

(5) $C_2H_5NO_2 = 75.07$ g/mol

$$\text{Required amount} = \frac{n_3 \times 75.07 \times 100}{99.5} = \mathbf{x_5'\ gm}$$

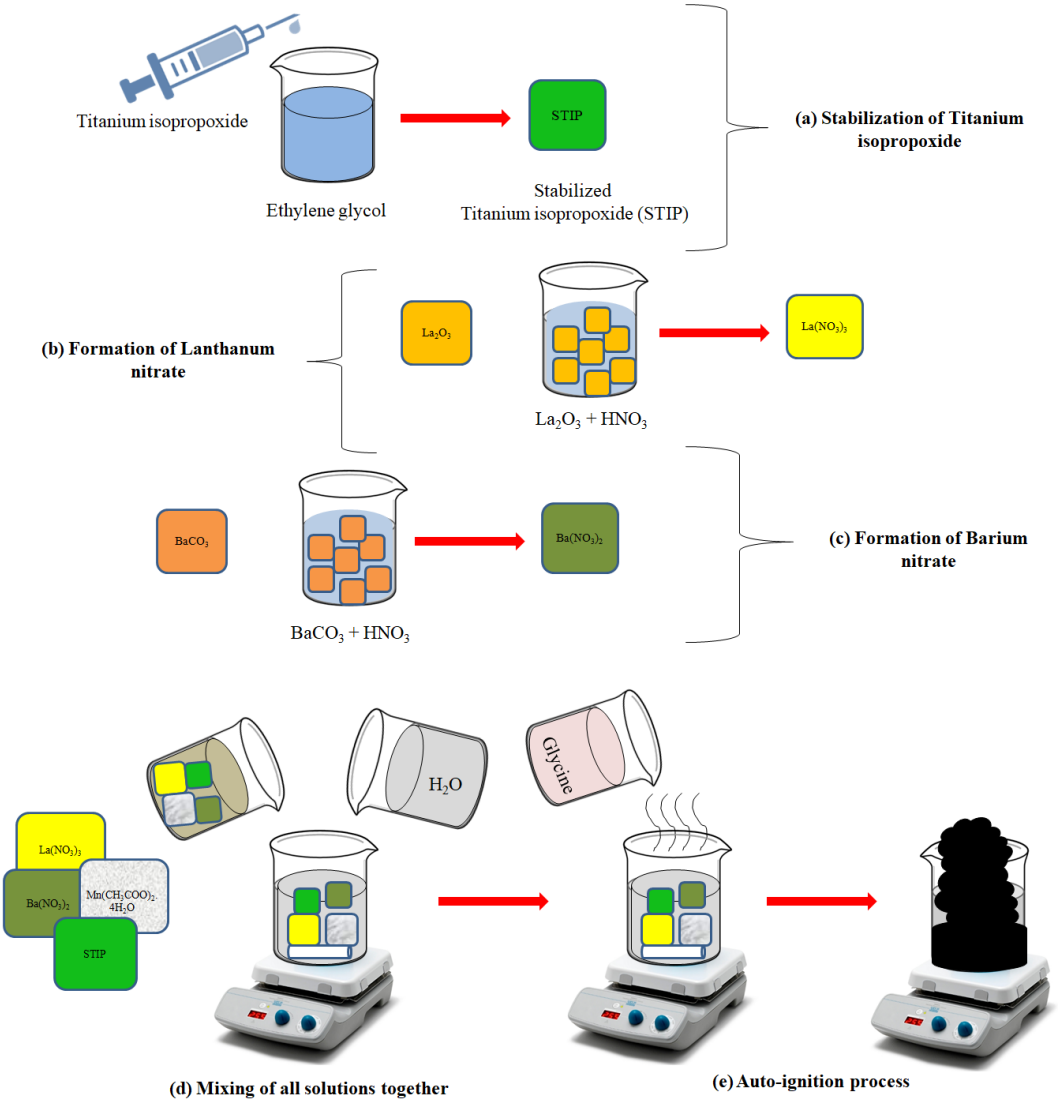

Figure 2.6: Schematic presentation of process for the synthesis of $La_{0.6}Ba_{0.4}Mn_{1-x}Ti_xO_3$ ($0.0 \leq x \leq 0.20$) perovskite manganites.

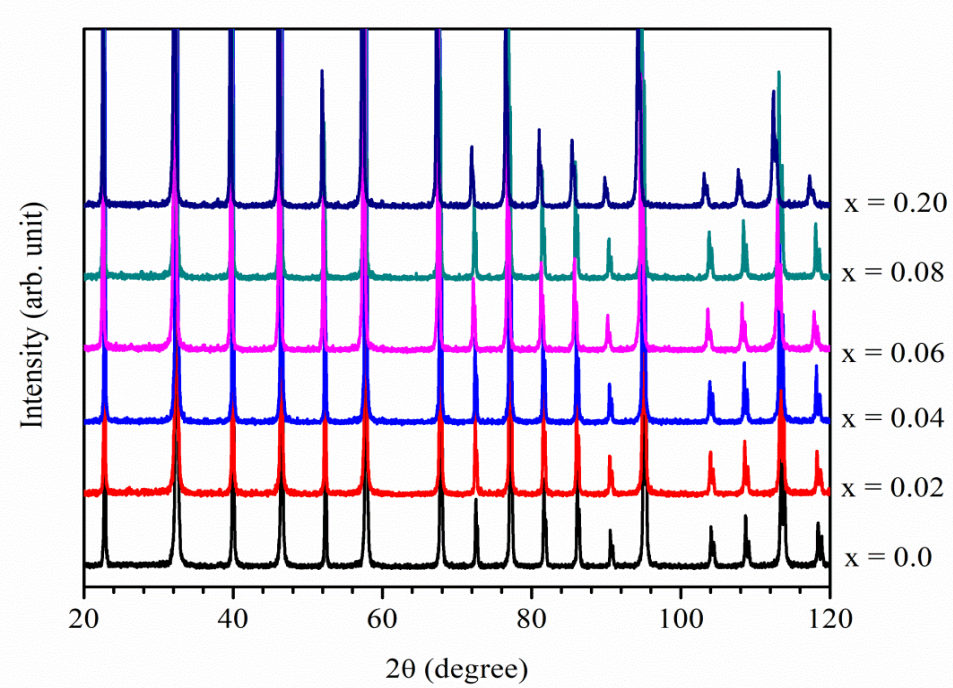

Figure 2.7: Room temperature XRD patterns of $La_{0.6}Ba_{0.4}Mn_{1-x}Ti_xO_3$ with x = 0, 0.02, 0.04, 0.06, 0.08 and 0.20 calcined at 1300°C temperature.

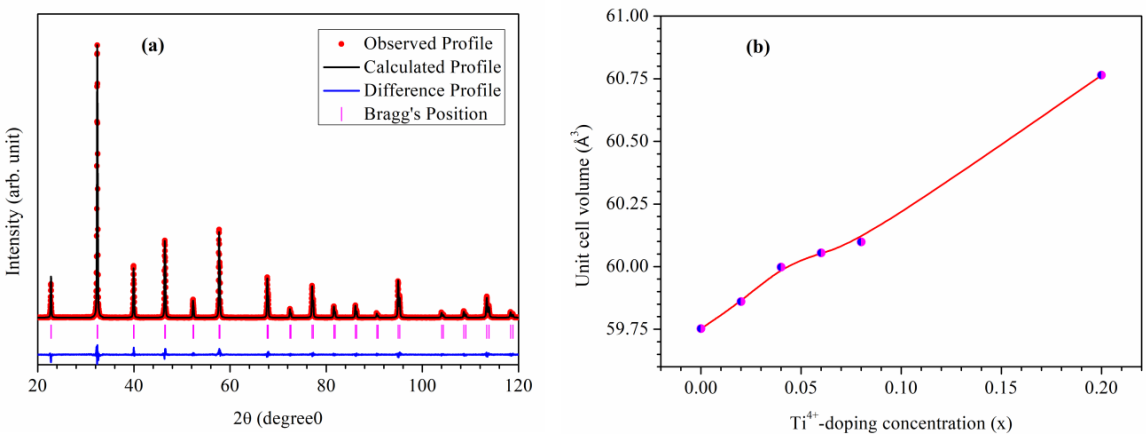

Figure 2.8: (a) Rietveld fit for XRD pattern of $La_{0.6}Ba_{0.4}Mn_{1-x}Ti_xO_3$ with x = 0 calcined at 1300°C temperature. (b) Variation in unit cell volume for $La_{0.6}Ba_{0.4}Mn_{1-x}Ti_xO_3$ as a function of Ti^{4+}-doping concentration (x).

2.6. Conclusions

The phase pure samples of the $Nd_{0.7}Ba_{0.3}Mn_{1-x}Ti_xO_3$ ($0 \leq x \leq 0.50$) and the $La_{0.6}Ba_{0.4}Mn_{1-x}Ti_xO_3$ ($0 \leq x \leq 0.20$) manganites have been synthesized using auto-combustion method. The parent sample of $Nd_{0.7}Ba_{0.3}Mn_{1-x}Ti_xO_3$ (x = 0.0) manganite has been calcined at 700, 800, 900, 1000, 1100 and 1200°C for 6 hrs to optimize to calcination temperature to produce a phase pure sample. The XRD patterns for $Nd_{0.7}Ba_{0.3}MnO_3$ samples calcined from 700-1100°C contain impurity phases. The XRD pattern for the sample of $Nd_{0.7}Ba_{0.3}MnO_3$ manganite calcined at 1200°C shows formation of pure phase. Hence, the $Nd_{0.7}Ba_{0.3}Mn_{1-x}Ti_xO_3$ manganites with $0 \leq x \leq 0.30$ were synthesized at 1200°C temperature, however, the samples with x = 0.40 and 0.50 were synthesized at 1350°C for 6 hrs. The $Nd_{0.7}Ba_{0.3}Mn_{1-x}Ti_xO_3$ (x = 0.10) manganite was calcined at 800, 900, 1000 and 1100°C for 6 hrs to synthesized samples of various particle sizes. The calcination temperature for the synthesis of pure phase of $La_{0.6}Ba_{0.4}Mn_{1-x}Ti_xO_3$ manganites with x = 0.0 was optimized and found to be 1300°C for 6 hrs. So, all the samples of $La_{0.6}Ba_{0.4}Mn_{1-x}Ti_xO_3$ manganites with ($0.0 \leq x \leq 0.20$) were synthesized at 1300°C. The phase purity of the $La_{0.6}Ba_{0.4}Mn_{1-x}Ti_xO_3$ manganites was checked by Rietveld analysis of the XRD patterns and found that $La_{0.6}Ba_{0.4}Mn_{1-x}Ti_xO_3$ manganites crystallize into single phase of cubic structure with $Pm\bar{3}m$ space group. The unit cell volume for $La_{0.6}Ba_{0.4}Mn_{1-x}Ti_xO_3$ manganites increases with increasing concentration of Ti^{4+}-ions.